Periodic orbits in coupled Hénon maps: Lyapunov and multifractal analysis

Antonio Politi
Instituto Nazionale di Ottica, I-50125 Firenze, Italy; INFN-Sezione di Firenze

Alessandro Torcini
Dipartimento di Fisica, Università di Firenze

(Received 4 May 1992; accepted for publication 20 July 1992)

A powerful algorithm is implemented in a 1-d lattice of Hénon maps to extract orbits which are periodic both in space and time. The method automatically yields a suitable symbolic encoding of the dynamics. The arrangement of periodic orbits allows us to elucidate the spatially chaotic structure of the invariant measure. A new family of specific Lyapunov exponents is defined, which estimate the growth rate of spatially inhomogeneous perturbations. The specific exponents are shown to be related to the comoving Lyapunov exponents. Finally, the ζ-function formalism is implemented to analyze the scaling structure of the invariant measure both in space and time.

I. INTRODUCTION

Various approaches have been devised in the past to describe low-dimensional chaotic attractors. The two most promising methods are based, respectively, on (i) the extraction of periodic orbits and the subsequent computation of a suitable dynamical ζ function;[1,2] (ii) symbolic encoding of the trajectories, detection of forbidden sequences and the construction of suitable directed graphs.[3] Knowledge of the symbolic dynamics, revealing the arrangements of the orbits onto hierarchical trees, is useful (essential) in either case, to increase the convergence of thermodynamic averages. Although the problem of finding an abstract and effective description of a strange attractor is, *per se*, a remarkable challenge, standard algorithms suffice, whenever just the estimate of either the fractal dimension, or a Lyapunov exponent is needed. However, the game is completely different, when dealing with relatively high-dimensional chaotic systems. There, the development of an approach ensuring a fast convergence is crucial also for the determination of rough reliable estimates.

Spatially extended systems provide perhaps the most prominent class of high-dimensional attractors. In this case, even a direct simulation can require prohibitively long CPU times. Coupled-map-lattice (CML) models have been invented to overcome part of the numerical difficulties.[4] A CML model can be essentially seen as the space–time discretization of a set of partial differential equations. Discretization of the time variable finds a justification in the procedure of constructing a Poincaré section for a flow. Space discretization, even if it cannot be rigorously justified, appears to be a reasonable assumption in all such cases where a physical cutoff is naturally appearing below a certain length scale. Moreover, it is an exact assumption in all systems inherently discrete (e.g., chains of coupled oscillators, arrays of Josephson junctions).

The most studied CML model is a 1-d chain of logistic maps, where the simplest chaotic maps are diffusively coupled to generate a large variety of spatio–temporal phenomena.[4] However, this dynamical system (and, more in general, all lattices involving maps of the interval) is characterized by a noninvertible dynamics, a property which can be hardly considered as realistic for a physical system. In order to overcome this difficulty, we have recently generalized the model, introducing a chain of coupled Hénon maps.[5] Throughout this paper, we will consider such a system as a test model for studying extended systems. A detailed analysis of the invariant measure is made possible by the implementation of an algorithm to extract all the orbits periodic both in space and time. This is based on the extension of a technique invented for the single Hénon map.[6]

Besides the analysis of short spatial chains, which clarify how the diffusive coupling affect the time evolution, we also look at the arrangements of the orbits of short time period for increasing space, very much in the same philosophy as in Eckmann and Procaccia.[7] For small coupling strength, it is shown the existence of a fully developed spatial chaos, which guarantees a fast convergence (in space) of thermodynamic averages.

The linear stability of generic trajectories is investigated in Sec. III with reference to perturbations exponentially growing (decaying) in space. This leads to the definition of *specific* Lyapunov exponents which depend on the spatial growth rate. The maximum specific Lyapunov exponent is shown to be the Legendre transform of the maximal comoving exponent,[8] and the same relation is conjectured to hold for the other exponents. This provides an alternative and more efficient way of computing the comoving Lyapunov exponents. Afterwards, the problem of estimating the Lyapunov spectrum of a spatially periodic orbit embedded in an infinite chain is investigated. The periodicity of the Jacobian allows us to reduce the problem to a finite dimensional one.

The knowledge of the Lyapunov spectra is finally exploited in Sec. IV, to compute appropriate ζ functions and determine the multifractal properties of dynamical entropies. This is done, by studying independently the temporal scaling (at fixed spatial length) and the spatial scaling (at fixed time length).

 1054-1500/92/030293-08$001.00

II. THE MODEL

The model of coupled Hénon maps is defined by

$$x_{t+1}^i = a - (y_t^i)^2 + b x_{t-1}^i, \tag{2.1}$$

with

$$y_t^i = \frac{\epsilon}{2} x_t^{i-1} + (1-\epsilon) x_t^i + \frac{\epsilon}{2} x_t^{i+1}, \tag{2.2}$$

where t and i denote time and space variables, respectively; a and b are the usual parameters of the Hénon map and ϵ is the diffusive coupling parameter. For $b=0$, Eqs. (2.1) and (2.2) reduce to those of the familiar lattice of logistic maps,[4] while for $\epsilon=0$, the evolution reduces to that of uncoupled Hénon maps. Notice that, for periodic boundary conditions, the Jacobian of map (2.1) is $(-b)^{\mathscr{I}}$, where $\mathscr{I}$ is the length of the chain. Therefore, the parameter b controls the dissipation exactly as it does in the single Hénon map. In particular, for $b=1$, a conservative dynamics is recovered. This set of properties establish the most serious justification for the choice of the coupling introduced in Eq. (2.1). Finally, one should notice that the dependence of the state variable at time $(t+1)$ on the state variable at two previous time steps prevents the simple interpretation of dynamics (2.1) as the composition of a local chaotic evolution with a diffusion process.

Whatever the method used to study chaos in a highly dimensional system, one is faced with the difficulty of collecting and dealing with a huge amount of information. In particular, a brute force approach is certainly hopeless if one is willing to extract periodic orbits. In fact, the Newton's method typically converges only in a small region around a given periodic orbit. Thus, one should generally iterate the map for a time long enough to pass sufficiently close to any cycle of interest. Moreover, one is never sure to have found all cycles of a given length. Here, we introduce a method which solves these difficulties for small values of the coupling strength ϵ.

The method is basically an extension of the approach introduced by Biham and Wenzel for the single Hénon map.[6] A fictitious dynamics is introduced along the continuous "time" axis τ,

$$x_t^i(\tau) = (-1)^{s(t,i)} [x_{t+1}^i(\tau) - a(y_t^i(\tau))^2 - b x_{t-1}^i(\tau)], \tag{2.3}$$

where the symbols $s(t,i) \in \{0,1\}$ have to be suitably chosen (the reason of their name will become clear in the following). Equation (2.3) is integrated by fixing periodic boundary conditions both in space and time ($x_{T+1}^i = x_1^i$, $x_0^i = x_T^i$, $x_t^{I+1} = x_t^1$, and $x_t^0 = x_t^I$). This means that any fixed point (in τ) corresponds to a spatio-temporal cycle (I,T) of period I in space and T in time. Notice that the choice of the $s(t,i)$ values does not affect the stationary property of a given solution, while one can expect it to affect its stability. Detailed numerical investigations have shown that the dynamical system (2.3) is characterized by the following properties: (i) any orbit (I,T) is stable for only one choice of the pattern of the $I \times T$ symbols $s(t,i)$; (ii) different periodic orbits are stable for different configurations of the $s(t,i)$'s. Accordingly, the $s(t,i)$'s provide a good symbolic representation of the dynamics generated by model (2.1). In particular, since such properties hold also for $b=0$, this approach can be also used to investigate the more familiar lattice of logistic maps.

A direct construction of the associated generating partition is practically unfeasible in a CML, since in a phase space of dimension $2I$ it requires the definition of a $2I-1$ dimensional volume. However, let us recall that in the single Hénon map (for the usual parameter values), the resulting partition coincides with that one directly constructed via the determination of homoclinic tangecies.[9]

The search of periodic orbits is further simplified by another property of model (2.1): in fact, a small coupling, apart from affecting the stability of the various orbits, essentially prunes out some of cycles which are present for $\epsilon=0$. Therefore, the knowledge of the topological structure of the single Hénon map allows us to restrict from the very beginning the set of symbol patterns to be investigated. As a matter of fact, an increasing, although small, number of exceptions to property (i) has been found when the coupling strength and the time period increase. For instance, for $a=1.4$, $b=0.3$, and $\epsilon=0.1$, less than 1% of failures has been detected for orbits up to temporal period 18. This is not a severe limitation, as this coupling strength is large enough to generate interesting phenomena.[10] Moreover, the few orbits missed by this technique can be identified through the implementation of a Newton's method tracing the orbits from the value of ϵ where they have been lost.

Among the spatio–temporal periodic orbits, we can find both stationary patterns and traveling waves. These two classes of solutions are clearly identified through their symbolic encoding. For instance, patterns like

$$\begin{pmatrix} 0 & 1 \\ 1 & 0 \end{pmatrix} \qquad \begin{pmatrix} 0 & 1 & 1 & 0 \\ 1 & 1 & 0 & 0 \\ 1 & 0 & 0 & 1 \\ 0 & 0 & 1 & 1 \end{pmatrix}$$

represent a same spatial string shifted by one step at each time. They would be seen as stationary patterns in a reference frame moving with velocity $v=1$. This argument introduces also the multiplicity of the various periodic patterns. In the case of a single map, the multiplicity of a given orbit (i.e., the number of different patterns obtained by shifting the symbolic sequence) coincides with the periodicity of the orbit itself. The above examples show that in the spatio–temporal case, the multiplicity does not simply coincide with the number IT of different symbols defining the pattern. In the first case, the multiplicity is 2 rather than 4 and in the second case, it is 4, rather than 16. An occurring discrepancy is also a way to distinguish between stationary patterns and traveling waves. In the latter case, the multiplicity is given by IT only in the appropriate reference frame, where the minimal time period is detected. We will return on this subject in Sec. IV, for the implementation of the ζ-function formalism.

A serious problem in reconstructing the statistical properties of an attractor from periodic orbits is to check whether all the orbits indeed belong to the natural invari-

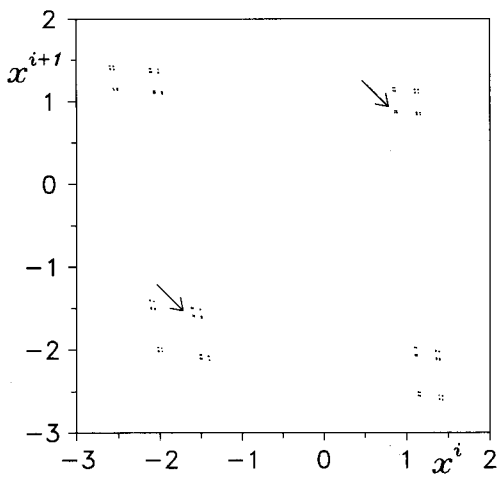

FIG. 1. Stationary periodic orbits of the model (2.1) for $a=1.4$, $b=.03$, and $\epsilon=0.2$. The arrows point to the fixed points of the single Hénon map.

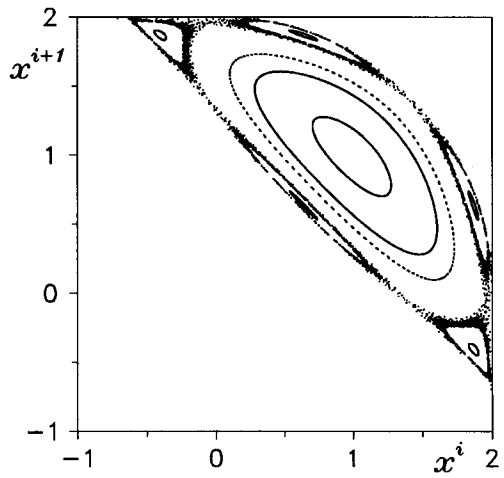

FIG. 2. Phase-space plot of map (2.4) for $b=0$, $a=2$, and $\epsilon=0.86$. The center of the tori is the fixed point of the logistic map $x_s=1$.

ant measure. For instance, in the single Hénon map, it is well known that one of the two fixed points is isolated and it does not belong to the strange attractor. Obviously, we expect that something similar should occur in the CML. In the case of coupled logistic maps, we know that the invariant measure is restricted to the interval delimited by the maximum of the map and its forward iterate. Therefore, any periodic orbit exhibiting at least one point out of such an interval must be discarded. This procedure finds a simple interpretation in the space of symbol sequences: any spatio–temporal periodic orbit characterized by a sequence of all 0's in at least one site has to be discarded (except for the special case $a=2$). The strict relation between logistic and Hénon maps suggests that the same rule applies in the latter case. Numerical simulations confirm this conjecture.

To further clarify this point we have plotted in Fig. 1 all stationary orbits up to period 8 in space. They are presented in the plane (x^i,x^{i+1}) for $\epsilon=.2$, and a Cartesian-product structure of two Cantor sets emerges. The two arrows point toward the fixed points of the single Hénon map; according to the previous considerations, only the positive one belongs to the invariant measure.

The representation adopted in Fig. 1 is justified by the fact that all stationary solutions are found by iterating in space Eqs. (2.1) and (2.2), once the time dependence has been dropped. Straightforward algebra shows that a 2-d map is obtained,

$$x^{i+1}=\frac{2}{\epsilon}(\pm\sqrt{a-(1-b)x^i}-(1-\epsilon)x^i)-x^{i-1}. \tag{2.4}$$

The Jacobian of this map is 1. This is a consequence of the invariance of model (2.1) under space reflection: accordingly, forward and backward iterations in space must be equivalent.

The periodic orbits plotted in Fig. 1 represent the skeleton of the invariant set associated with map (2.4). Such a map has the unpleasant property of being ill-defined because of the sign indeterminacy in front of the square root. However, this difficulty, which should not arise in a realistic physical system, is easily removed if one interprets Eq. (2.1) as the limit case ($\delta\to 0$) of the more general model

$$x^i_{t+1}=a-(y^i_t)^2+bx^i_{t-1}+\delta(y^{i-1}_t+y^{i+1}_t), \tag{2.5}$$

where a next-to-nearest neighbor coupling has been added. The spatial map describing the stationary solutions of Eq. (2.5) can be written in a compact form, by exploiting Eq. (2.2),

$$x^{i+1}=\frac{2}{\epsilon}(y^i-(1-\epsilon)x^i)-x^{i-1},$$

$$y^{i+1}=\frac{2}{\delta}((1-b)x^i-a-(y^i)^2)-y^{i-1}. \tag{2.6}$$

We can see that, at the expense of doubling the phase-space dimension, the sign indeterminacy has disappeared. It can be interpreted as the effect of the strong expansion due to the multiplier $2/\delta$ appearing in the second equation of Eq. (2.6). The fluctuating sign is essentially the mechanism which leads to the Cantor-like structure seen in Fig. 1. However, one might ask whether, besides this mechanism, the nonlinearity of map (2.4) can, *per se*, give rise to spatial chaos. The simplest step in this direction, is represented by the stability analysis of map (2.4) for fixed sign (i.e., spatial stability of the two homogeneous solutions). Straightforward calculations show that the eigenvalues become purely complex above the critical value

$$\epsilon_c=\tfrac{1}{2}+(1-b)/4x_s, \tag{2.7}$$

where x_s represents the stationary solution (for the logistic maps at $a=2$, $\epsilon_c=3/4$). Above the critical value, spatially quasiperiodic solutions should appear around the fixed point. Moreover, since a 2-d conservative map is not in general integrable, a chaotic structure should be present as well. This is confirmed by the numerical iteration of Eq. (2.4) for $b=0$, $a=2$, and $\epsilon=0.86$. The results of the simulations, reported in Fig. 2, are the typical picture obtained for a nearly integrable Hamiltonian system.

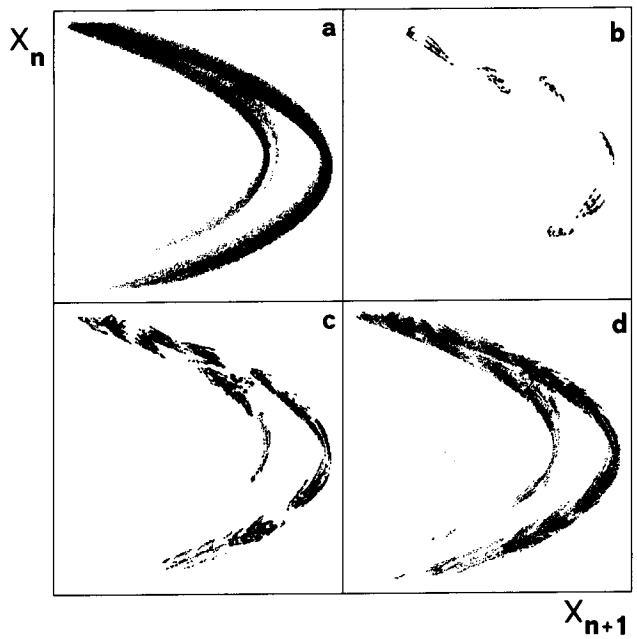

FIG. 3. Projection of the invariant measure onto the local space x^i_{n+1}, x^i_n. In (a) the result of a direct iteration of a chain of 1000 maps is reported; in (b), (c), and (d) periodic orbits up to period (3,9), (4,7), and (5,4), respectively, are reported.

It is important to notice that all the trajectories reported in Fig. 2 are characterized by a positive x^i. As they are, by construction, stationary solutions, it turns out that the simple partition—defined for logistic maps by associating either 0 or 1 to the site (i,t), according to the sign of x^i_t—is not (at least in this parameter range) a generating partition. In fact, all such trajectories would be encoded in the same way. Another important point to observe is that in the region $\epsilon > \epsilon_c$, the birth of spatially quasiperiodic solutions indicates that an increase of the coupling strength corresponds to an increase in the number of orbits and presumably an increase of the topogical entropy.

A complementary and more standard representation is presented in Fig. 3, where x^i_t is plotted vs x^i_{t+1}. In Fig. 3(a) the result of the direct iteration of model (2.1) is reported for $\epsilon=0.075$. The resemblance with the Hénon attractor is evident. In Figs. 3(b), 3(c), and 3(d), the same representation is adopted to plot the orbits of period (I,T) up to (3,9), (4,7), and (5,4), respectively. All the points clearly fall inside the region visited by the direct simulation.

III. LYAPUNOV ANALYSIS

The linear stability analysis of strange attractors concerns the problem of measuring the divergence in time of nearby trajectories. In extended systems, the spatial dependence of the state variable leads also to propagation phenomena and, more in general, to spatial inhomogeneities.

Various dynamical indicators have been introduced to characterize the different effects. In particular, two complementary approaches have been developed based, respectively, on the temporal (spatial) growth rate of given space (time) periodic perturbations. The former approach is the standard method to determine the spectrum of Lyapunov exponents. The latter one, which leads to the spatial Lyapunov exponents is useful both in revealing the localization properties of Lyapunov vectors[11] and characterizing the stability properties in open-flow systems (i.e., systems with an asymmetric spatial coupling).[12] Still another approach, conceived to quantify the growth rate of a disturbance in a moving reference frame, has been developed by Deissler and Kaneko,[8] who introduced the so-called comoving Lyapunov exponents. This last technique can be seen as a sort of combination of the previous ones.

A general question naturally arises as to whether such indicators are really independent from one another and whether they guarantee an exhaustive description of all possible instabilities. In the following we make a first step in this direction by showing that the introduction of more general boundary conditions leads to define a wider class of Lyapunov exponents (specific exponents) which are in fact related to the comoving exponents.

Let us start from the linear stability problem for a chain of Hénon maps. In model (2.1), we have chosen periodic boundary conditions in view of the characterization of spatio–temporal chaos in terms of periodic orbits. In the tangent space, it is useful to assume a more general spatial dependence of the perturbation, namely, $\delta^i_t = e^{\mu i} u^i_t$, where μ is an exponential spatial growth rate and where periodic boundary conditions are assumed for u^i_t (i.e., $u^{\mathscr{I}+1}_t = u^1_t$, $u^0_t = u^{\mathscr{I}}_t$). The evolution of u^i_t is ruled by the equation

$$u^i_{t+1} = -2y^i_t \left[\frac{\epsilon}{2} e^{-\mu} u^{i-1}_t + (1-\epsilon) u^i_t + \frac{\epsilon}{2} e^{\mu} u^{i+1}_t \right] + b u^i_{t-1}. \tag{3.1}$$

Iteration of Eq. (3.1) allows the computation of the specific Lyapunov exponents $\lambda_j (1 \leqslant j \leqslant 2\mathscr{I})$ which measure the time stability of exponentially spatially increasing (decreasing) perturbations. For $\mu=0$, strictly periodic boundary conditions are recovered also for the perturbation and the standard Lyapunov exponents are recovered.

In general, we expect that the Lyapunov exponents scale as

$$L(\rho = j/\mathscr{I}, \mu) = \lambda_j(\mu) \tag{3.2}$$

for a sufficiently long chain length I.[13]

An alternative approach to the stability of spatial systems is based on the so-called comoving Lyapunov exponents. They are defined in terms of the growth rate of an initial perturbation δ^i_0 spread over the finite interval $-L_0/2 \leqslant i \leqslant L_0/2$. Due to the nearest-neighbor coupling, the disturbance remains confined to the light cone $-L_0/2 - t < i < L_0/2 + t$. Previous numerical analyses indicate that for t sufficiently long,

$$|\delta^i_t| \simeq e^{\Lambda(i/t)t}, \tag{3.3}$$

where Λ, the maximal comoving Lyapunov exponent,[8] is a function of $v = i/t$ only. Hence, $\Lambda(v)$ represents the time growth rate of the perturbation in a frame moving with velocity v. Notice that the limit $t \to \infty$ (required by a meaningful definition of Λ) implicitely requires the infinite-

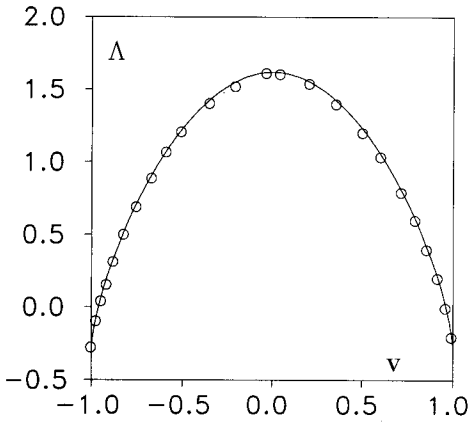

FIG. 4. Maximal comoving Lyapunov exponent Λ vs the velocity v. The dots refer to the direct estimate from Eq. (3.3); the line is obtained by taking the Legendre transform of $\lambda(\mu)$ [defined in Eq. (3.4) and computed by iterating Eq. (3.1)].

chain limit and that the initial width L_0 of the disturbance is not a relevant parameter. This is no longer true when the whole spectrum of comoving exponents is investigated, since L_0 is related to the dimension of the tangent space of interest.[8]

From Eq. (3.3) it is clear that the spatial profile of the perturbation is locally exponential. Indeed, by considering two nearby sites and expanding Λ, we obtain

$$\Lambda\left(\frac{i+1}{t}\right)\simeq\Lambda\left(\frac{i}{t}\right)+\Lambda'\left(\frac{i}{t}\right)\frac{1}{t}, \tag{3.4}$$

where the prime denotes the derivative with respect to the argument. From the definition of spatial exponent, $\mu=\log(\delta_t^{i+1}/\delta_t^i)$, and from Eqs. (3.3) and (3.4), we obtain

$$\mu=\Lambda'(v). \tag{3.5}$$

The locally exponential shape of the perturbation indicates that the temporal growth rate at fixed site is simply the previously defined specific exponent $\lambda(\mu)$, namely,

$$|\delta_{t+T}^i|\simeq|\delta_t^i|e^{\lambda(\mu)T} \tag{3.6}$$

provided that T is sufficiently long and μ does not change appreciably between t and $t+T$ in the site i. It is readily seen that the latter condition is satisfied for $T\ll t$. From Eqs. (3.3) and (3.6), and after expanding Λ around $v=i/t$, we find

$$\lambda(\mu)=\Lambda(v)-v\Lambda'(v). \tag{3.7}$$

Equations (3.5) and (3.7) show that the comoving exponent $\Lambda(v)$ is linked to the specific exponent $\lambda(\mu)$ through a Legendre transform. Such a transformation generalizes the result of Ref. 14, where it was derived in the case of a linear equation with constant coefficients, following a somewhat different approach, based onto dispersion relations. We have tested Eqs. (3.5) and (3.7) for randomly generated coefficients y_t^i. The outcomes of numerical simulations are reported in Fig. 4, where the dots refer to the direct estimate of the comoving exponent, while the continuous line is the result of the Legendre transform. The very good agreement confirms the correctness of the assumptions made in the derivation of Eqs. (3.5) and (3.7). It is natural to conjecture that the other comoving exponents are related in the same way to the specific exponents obtained from Eq. (3.1).

From now on, we restrict the analysis to the standard case $\mu=0$ and discuss the computation of Lyapunov exponents of orbits periodic both in space and time. This is an important problem, recalling that periodic orbits are essential ingredients to estimate the Taylor expansion of dynamical ζ functions. In the limit of an infinitely extended system ($\mathscr{I}\to\infty$), even the stability analysis of an orbit with finite spatial period I must be carried out in an infinite-dimensional space. Such an additional difficulty can be partly overcome by exploiting the spatial periodicity of the orbit under investigation. Indeed, in the following, we show that the Floquet theorem allows us to reduce the dimensionality of the space to $2I$. This method is analogous to that one devised in Ref. 12, where "quasi-Lyapunov" exponents have been introduced to describe the spatial stability of time periodic oscillations, which are stationary in space (i.e., space and time variables are interchanged).

We first rewrite Eq. (3.1) in vector notations,

$$\begin{pmatrix}\mathbf{u}_{t+1}\\ \mathbf{z}_{t+1}\end{pmatrix}=J_t\begin{pmatrix}\mathbf{u}_t\\ \mathbf{z}_t\end{pmatrix}, \tag{3.8}$$

where the Jacobian J_t is the spatially periodic operator

$$J_t=\begin{pmatrix}\Phi_t\Gamma & bE\\ E & 0\end{pmatrix},$$

Φ_t is a diagonal matrix such that $(\Phi_t)_{ii}=-2y_t^i$, Γ is the tridiagonal symmetric matrix responsible of the diffusive coupling, and E is the identity matrix.

In the case of a stationary solution, Φ_t and, in turn, J_t are independent of t and the stability of the orbit is deduced from the eigenvalues of J (we can drop the dependence on t). According to the Floquet theorem, the eigenvectors $(\mathbf{v},\mathbf{w})$ of J can be expressed as (j being the imaginary unit)

$$v^i(l,k)=e^{jki}v_{(p)}^i(l,k),\quad w^i(l,k)=e^{jki}w_{(p)}^i(l,k), \tag{3.9}$$

where the wave number k is equal to $2\pi\phi\mathscr{I}$ ($0\leqslant\phi\leqslant1$), l is the band index ($1\leqslant l\leqslant 2I$), and $v_{(p)}$, $w_{(p)}$ are periodic functions of i. By substituting Eq. (3.9) in the eigenvalue problem for J, we find

$$\begin{aligned}mv_{(p)}^i&=-y^i[2(1-\epsilon)v_{(p)}^i\\&\quad+\epsilon(e^{-jki}v_{(p)}^{i-1}+e^{+jki}v_{(p)}^{i+1})]+bw_{(p)}^i,\\ mw_{(p)}^i&=v_{(p)}^i,\end{aligned} \tag{3.10}$$

where m is an eigenvalue, and the dependence on l and k has been dropped for the sake of simplicity. For each choice of the wave number k, $2\mathscr{I}$ eigenvalues are found by solving the linear system (3.10). The Lyapunov exponents are then given by $\log|m|$ ($|\cdot|$ denotes the modulus oper-

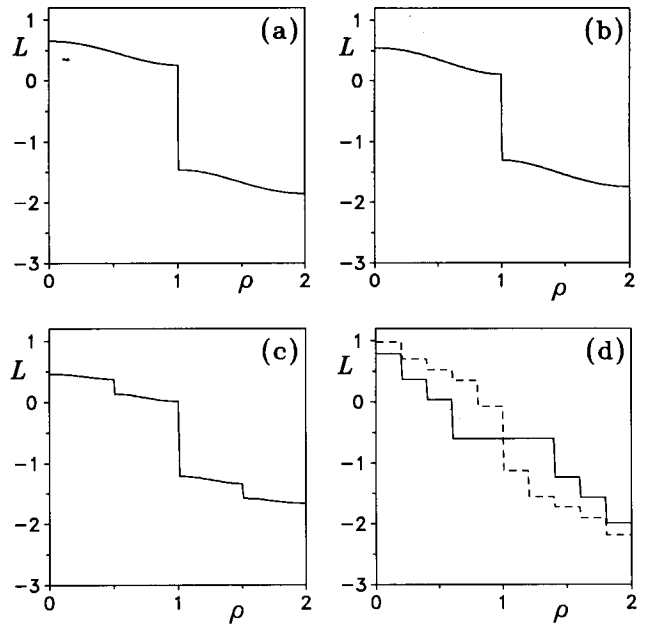

FIG. 5. Lyapunov spectra L of the map (2.1) for some spatio–temporal periodic orbits (I,T): (1,1) (a), (1,9) (b), (2,7) (c), (4,5) (d). The two curves appearing in (d) refers to two distinct spatio–temporal cycles (4,5). L is reported as a function of the continuous variable ρ.

ation), and the spectrum $L(\rho)$ is determined after ordering the various bands, and taking into account possible overlaps.

The extension to orbits also periodic in time is straightforward. It is sufficient to introduce again the dependence on t in Eq. (3.10) (through y_t) and iterate it T times. In other words, we must calculate the product $\tilde{J}_T=\Pi_{t=1}^{T} J_t(k)$, where $J_t(k)$ is the operator implicitely defined in the r.h.s. of Eq. (3.10). The Lyapunov exponents are then given by $\log|m_T|/T$, where the m_T's are the eigenvalues of $\tilde{J}_T(k)$. Accordingly, the infinite-dimensional problem of determining the Lyapunov spectrum of a spatio–temporal periodic orbit is reduced to that of finding the eigenvalues of $2\mathscr{I}\times 2\mathscr{I}$, matrices.

However, an analytic estimate of the spectrum cannot be generally found even for periodic solutions. In the case of a stationary and spatially homogeneous solution $x_t^j=\bar{x}$, this is possible, and the solution is

$$e^{L_\pm(\rho)}=-\bar{x}(1-2\epsilon\sin^2(\pi\rho/2))\times\left[1\pm\sqrt{1+\frac{4b}{4\bar{x}^2(1-2\epsilon\sin^2(\pi\rho/2))}}\right]. \tag{3.11}$$

This expression generalizes the result of Ref. 15, determined for logistic maps. The spectrum (3.11) is also reported in Fig. 5(a) for $\epsilon=0.075$. The two bands L_+ and L_- arise from the two Lyapunov exponents of the single Hénon map, to which they reduce for $\epsilon=0$. A small diffusive coupling removes the degeneracy, leading to two thin bands. The spectra of other spatio–temporal periodic orbits are also reported in Fig. 5, the number of distinct bands being connected with the spatial periodicity. Notice that the number of states characterized by a positive Lyapunov exponents depends on the orbit, and this represents a new feature arising in extended systems which makes the structure of the invariant measure still more intriguing.[5,16]

IV. MULTIFRACTAL ANALYSIS

The computation of Lyapunov exponents, fractal dimensions, and metric entropies require to construct—either implicitely, or explicitely—increasingly fine partitions of the phase-space. This can be done in a natural way by exploiting symbolic dynamics. Each element S_j of the partition is defined as the set of the points generating trajectories which are characterized by the same given symbols both in the future (f) and in the past (p). The numbers f,p control the size of S_j along the unstable, resp. stable manifold. The measure $\mathscr{P}_j$ of the element S_j (i.e., the probability to observe a given symbol sequence of length $T=p+1+f$) can be shown to scale as[17]

$$\mathscr{P}_j\simeq e^{-H_jT}, \tag{4.1}$$

where H_j is the sum of all positive Lyapunov exponents. Since, in the case of spatio–temporal chaos, the dynamical entropy H_j is an extensive quantity,[13,18] it is convenient to introduce the intensive variable $h_j=H_j/\mathscr{I}$. In the thermodynamic limit ($\mathscr{I}\to\infty$), the entropy density h_j is thus expressed in terms of an integral of the Lyapunov spectrum,

$$h_j=\int L_j(\rho)d\rho, \tag{4.2}$$

where the integration extends over positive L_j's. An analogous expression can be written for the local dimension density (see Ref. 5).

We are now in the position to apply the thermodynamic formalism to characterize the invariant measure. Typically, one has to determine the scaling behavior of a sum of variables R_j's (e.g., multipliers, box sizes) associated with the elements of a given partition (that is the trajectories of length T or, equivalently, orbits of period T),

$$\sum_j R_j\simeq e^{\beta T}. \tag{4.3}$$

One of the most effective approaches to determine β is the ζ-function method, developed along the lines of the grand-canonical formalism. After multiplying Eq. (4.3) by the factor z^T and summing over T, we arrive, with some algebraic manipulations, at the dynamical ζ function[1]

$$\zeta^{-1}(z)=\prod_j (1-z^TR_j^T)^{m_j}, \tag{4.4}$$

where the product is extended to orbits distinct under temporal rotations. The multiplicity m_j denotes the number of the different trajectories identified by the same value R. In fact, we have seen in Sec. II that translational invariance (as well as reflection symmetry) implies the existence of classes of orbits characterized by the same Lyapunov exponents. The rate β is implicitely given by the first zero of

$$\zeta^{-1}(\log\beta)=0. \tag{4.5}$$

While the exact evaluation of ζ requires the knowledge of an infinity of orbits, a truncation of its Taylor expansion guarantees, in many cases, an accurate determination of β.[2]

So far, we have mainly summarized the formalism as it was developed for low-dimensional chaos. In the case of a CML, the factors R_j depend exponentially both on space and time variables ($R_j \simeq r_j^{T\mathscr{I}}$). This suggests that the ζ-function formalism could be effectively extended, by performing an additional sum over all spatial periods. Unfortunately, a straight implementation of this scheme is not so effective as in the low-dimensional case. Therefore, we limit ourselves to apply the standard formalism, checking afterwards the dependence on the length chain $\mathscr{I}$.

Let us consider the generalized entropy densities $l(q)$, defined by

$$\sum_j e^{-h_j\beta T\mathscr{I}} \simeq e^{l(q)T\mathscr{I}}, \tag{4.6}$$

where the sum is extended over the primitive orbits of period T in time and $\mathscr{I}$ in space (and their submultiples), while h_j is the local entropy density in a chain of length $\mathscr{I}$. One should observe that the scaling assumption implicitely made in (4.6), as all the analogous assumptions made throughout this paper are strictly referred to closed systems, where no flow of information comes through the boundaries, in which case the expected scaling dependence would be less clear.[19]

An equivalent, but more enlightening presentation of the generalized entropies is provided by the Legendre transform of $l(q)$,[20]

$$g_t(h)=hq-l(q), \quad h=l'(q). \tag{4.7}$$

The comparison of Eq. (4.6) with Eq. (4.3), indicates that $l(q)$ and in turn $g_t(h)$ can be determined by introducing an appropriate ζ function.

Since T and $\mathscr{I}$ play a perfectly symmetric role, we can alternatively develop the ζ-function formalism by fixing the time period T, and letting $\mathscr{I}$ diverge to ∞. This approach is perfectly complementary to the standard one. It is more suited in accounting for the spatial coherence, while less effective for what concerns the temporal convergence. Let us define the spectra obtained from these two approaches as the temporal ($g_t(h)$) and the spatial ($g_s(h)$) spectrum, respectively. However, assuming that the limits $\mathscr{I}\to\infty$ and $T\to\infty$ do commute, we expect that

$$\lim_{\mathscr{I}\to\infty} g_t(h) = \lim_{T\to\infty} g_s(h). \tag{4.8}$$

The results of numerical simulations for $a=1.4$, $b=0.3$, and $\epsilon=0.075$ are illustrated in Figs. 6 and 7, where temporal, reps. spatial spectra have been reported. The spectrum $g_t(h)$ of a chain of length $\mathscr{I}=2$ has been obtained by truncating the expansion of ζ^{-1} after 18 terms (i.e., considering all orbits up to period $T=18$). It almost coincides with the spectrum for $\mathscr{I}=3$ (obtained with $T=15$), revealing a fast convergence for increasing chain length $\mathscr{I}$.

The spatial spectra $g_s(h)$ reported in Fig. 7 correspond to temporal periods $T=7$, 8, and 9. They have been obtained, by considering all orbits of spatial period $\mathscr{I}=6$, 4, and 5, respectively. The comparison between the spectra obtained for increasing $\mathscr{I}$ (i.e., successive truncations of the ζ function) indicates that the spatial convergence is very fast, thus allowing us to arrive at such long time periods. On the other hand, the relatively large differences among the three spectra of Fig. 7 indicate a slow convergence in time. We have encountered the same difficulty in the computation of the temporal spectrum, where a good convergence for $g_t(h)$ is achieved only considering a large number of terms ($T\geqslant 15$). However, the reasonable agreement between $g_s(h)$ for $T=9$ and $g_t(h)$ for $\mathscr{I}=3$ suggests that such spectra are not far from the asymptotic limit, when Eq. (4.8) holds.

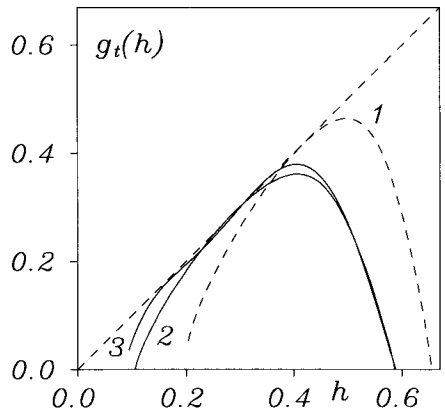

FIG. 6. Multifractal temporal spectra of entropy density $g_t(h)$ for $a=1.4$, $b=0.3$, and $\epsilon=0.075$. The numbers denote the chain lengths corresponding to the different spectra. The spectrum of the single map (dashed line) coincides with that of the CML for $\epsilon=0$.

Finally, the multifractal analysis allows us to clearly reveal the stabilizing effect of the diffusive coupling ϵ. Indeed, the comparison between the spectrum of the single map (which coincides with the spectrum of the CML for $\epsilon=0$) and those obtained for 2 and 3 coupled maps (see Fig. 6) indicates that the latter ones are restricted to

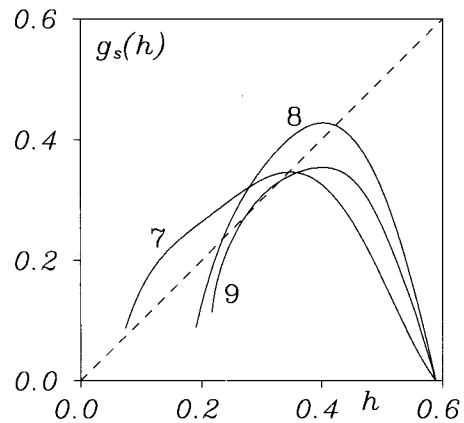

FIG. 7. Multifractal spatial spectra of entropy density $g_s(h)$ for $a=1.4$, $b=0.3$, and $\epsilon=0.075$. The numbers denote the temporal period corresponding to each spectrum.

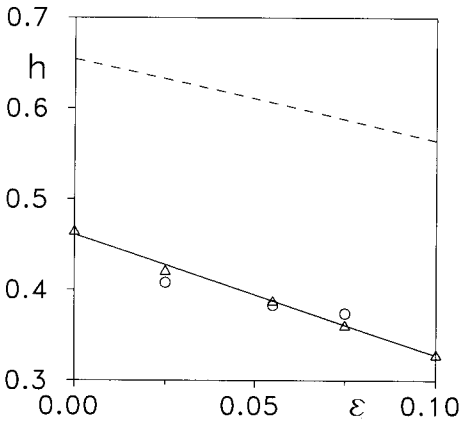

FIG. 8. Entropy densities vs the coupling parameter ϵ. The dashed lines refers to the maximum entropy density, computed from the spectrum given in Eq. (3.11). Triangles and circles denote the topological entropy density for a chain length $\mathscr{I}=2$, 3, respectively. The solid line represents a linear fit obtained from the data for $\mathscr{I}=2$.

smaller entropy values. The effect of the diffusive coupling is better elucidated by investigating the dependence of the topological entropy density $l(0)$ on ϵ. In Fig. 8, $l(0)$ is reported for different ϵ values (triangles and circles refer to 2, 3 maps, respectively). The numerical results indicate a linear decrease of the topological entropy density for small values of ϵ. For comparison, we have also reported the behavior of the maximum entropy density (dashed line). The maximum is obtained in correspondence of the stationary homogeneous orbit and has been computed from Eqs. (4.2) and (3.11). Its behavior confirms the linear decrease displayed by $l(0)$ for $\mathscr{I}=2,3$.

[1] D. Ruelle, *Statistical Mechanics, Thermodynamic Formalism* (Addison-Wesley, Reading, MA, 1978).
[2] P. Cvitanovič, Phys. Rev. Lett. **16**, 2729 (1988).
[3] J. P. Crutchfield and K. Young, Phys. Rev. Lett. **63**, 105 (1989); G. D'Alessandro, P. Grassberger, S. Isola, and A. Politi, J. Phys. A **23**, 5285 (1990).
[4] K. Kaneko, Prog. Theor. Phys. **72**, 480 (1984); R. Kapral, Phys. Rev. A **31**, 3868 (1985).
[5] A. Politi and A. Torcini, Towards a Statistical mechanics of spatio–temporal chaos, preprint, 1992.
[6] O. Biham and W. Wenzel, Phys. Rev. Lett. **63**, 819 (1989).
[7] J.-P. Eckmann and I. Procaccia, Phys. Rev. Lett. **66**, 891 (1991).
[8] R. J. Deissler and K. Kaneko, Phys. Lett. A **119**, 397 (1987).
[9] P. Grassberger, H. Kantz, and U. Moenig, J. Phys. A **43**, 5217 (1989).
[10] See J. P. Crutchfield and K. Kaneko, in *Directions in Chaos*, edited by H. Bao-Lin (World Scientific, Singapore, 1987), p. 272, for the chain of logistic maps.
[11] G. Giacomelli and A. Politi, Europhys. Lett. **15**, 387 (1991).
[12] A. S. Pikowsky, Phys. Lett. A **137**, 121 (1989).
[13] Y. Pomeau, A. Pumir, and P. Pelce, J. Stat. Phys. **37**, 39 (1984); K. Kaneko, Prog. Theor. Phys. **74**, 1033 (1984); P. Manneville, in *Lectures Notes in Physics*, Vol. 230 (Springer, Berlin, 1985), p. 319; R. Livi, A. Politi, and S. Ruffo, J. Phys. A **19**, 2033 (1986).
[14] T. Bohr and D. Rand, A mechanism for localized turbulence, preprint, 1987.
[15] S. Isola, A. Politi, S. Ruffo, and A. Torcini, Phys. Lett. A **143**, 365 (1990).
[16] A Pikovski and P. Grassberger, Symmetry breaking bifurcation for coupled chaotic attractors, preprint WU B91-18, Wuppertal, 1991.
[17] P. Grassberger, R. Badii, and A. Politi, J. Stat. Phys. **51**, 135 (1988).
[18] P. Grassberger, Physica Scripta **40**, 346 (1989).
[19] A. Politi and G. Puccioni, Physica D (to be published).
[20] R. Benzi, G. Paladin, G. Parisi, and A. Vulpiani, J. Phys. A **18**, 2157 (1985); T. C. Halsey, M. H. Jensen, L. P. Kadanoff, I. Procaccia, and B. Shraiman, Phys. Rev. A **33**, 1141 (1986).